Earth and Planetary Science Letters 578 (2022) 117341

Contents lists available at ScienceDirect

Earth and Planetary Science Letters

www.elsevier.com/locate/epsl

Controlling factors and impacts of river-borne neodymium isotope signatures and rare earth element concentrations supplied to the Canadian Arctic Archipelago

M. Grenier [a,*], K.A. Brown [b], M. Colombo [c], M. Belhadj [a], I. Baconnais [d], V. Pham [a], M. Soon [c], P.G. Myers [e], C. Jeandel [a], R. François [c]

[a] LEGOS, University of Toulouse, CNRS, CNES, IRD, UPS, Toulouse, 31400, France
[b] Fisheries and Oceans Canada, Institute of Ocean Sciences, Sidney, BC, Canada
[c] Department of Earth, Ocean, and Atmospheric Sciences, University of British Columbia, Vancouver, Canada
[d] Saskatchewan Isotope Laboratory, Department of Geological Sciences, University of Saskatchewan, Saskatoon, Canada
[e] Department of Earth and Atmospheric Sciences, University of Alberta, Edmonton, Alberta, Canada

ARTICLE INFO

Article history:
Received 12 February 2021
Received in revised form 7 December 2021
Accepted 10 December 2021
Available online 17 December 2021
Editor: A. Jacobson

Keywords:
river geochemistry
Rare Earth Elements
neodymium isotopes
bedrock geology
dissolved riverine inputs
Canadian Arctic Archipelago

ABSTRACT

Determining the factors controlling the neodymium (Nd) isotopic compositions (expressed as ε_{Nd}) and rare earth element (REE) concentrations of rivers is imperative to improve our understanding of the distribution of these water mass tracers in the ocean. Here we present the first measurements of <0.45 µm-filtrate REE concentrations (i.e., the concentration of truly dissolved, nano-particulate and colloidal REEs passing through a 0.45 µm filter, hereafter referred to as dissolved) and ε_{Nd} in rivers draining into the Canadian Arctic Archipelago (CAA). Results show a large variation in both REE concentrations (Nd = [8; 37, 260] pmol/kg) and ε_{Nd} ([−32.1; −15.1]) in the thirteen rivers sampled. Dissolved REE concentrations increase with increasing fractions of metamorphic rocks and ice cover in the rivers' watersheds, while ε_{Nd} and PAAS-normalized REE patterns are inherited from the watershed's bedrock lithology. The four rivers draining watersheds composed of Precambrian metamorphic rocks exhibit the highest REE concentrations, the least radiogenic ε_{Nd}, and shale-normalized patterns enriched in light REEs. The remaining nine rivers drain mainly or exclusively sedimentary bedrock and have lower REE concentrations, more radiogenic ε_{Nd} and generally show heavy REE enrichment, with variable negative cerium (Ce) anomalies. The presence of ice sheets in the drainage area, and the ionic strength, pH, and dissolved organic carbon concentration of river water are the main factors determining riverine dissolved REE concentrations by controlling the formation and stabilization of colloids. We estimate a flow of dissolved Nd transported by Arctic rivers discharging into the CAA equivalent to the Nd flux of seawater entering the CAA. Depending on the percentage of Nd removal during mixing with seawater, the impact of river water on the ε_{Nd} of seawater exiting the CAA could be modest (if 90% removal) or more significant (if ≪90% removal). This riverine contribution could potentially impart a climate-sensitive ε_{Nd} signature to the seawater reaching Baffin Bay, with possible implications for the use of ε_{Nd} in paleoceanographic reconstructions of water mass distribution.

© 2021 The Author(s). Published by Elsevier B.V. This is an open access article under the CC BY-NC-ND license (http://creativecommons.org/licenses/by-nc-nd/4.0/).

1. Introduction

The distribution of neodymium isotopes in the world ocean suggests that seawater acquires its Nd isotopic composition (ε_{Nd}[1]) from the continental margins (Jeandel et al., 2007). The dominance of older granitic rocks surrounding the North Atlantic would impart a comparatively unradiogenic ε_{Nd} to North Atlantic water and to deep water masses formed in this region, while the younger volcanic rocks dominating the Pacific margins would impart a more radiogenic signature to Pacific water. This contrast between the ε_{Nd} of seawater in the Atlantic and Pacific Ocean has been used in paleoceanography to reconstruct past changes in water mass distribution (Frank, 2002). One of the basic assumptions in this application is that the ε_{Nd} tagging of the two end member water masses remains unchanged through time. However, the exact

* Corresponding author.
E-mail address: melanie.grenier@legos.obs-mip.fr (M. Grenier).

[1] $\varepsilon_{Nd} = [(^{143}Nd/^{144}Nd)_{SAMPLE}/(^{143}Nd/^{144}Nd)_{CHUR} - 1] \times 10^4$, where $(^{143}Nd/^{144}Nd)_{CHUR} = 0.512638$ (Wasserburg et al., 1981). CHUR, Chondritic Uniform Reservoir; present day average Earth value.

https://doi.org/10.1016/j.epsl.2021.117341
0012-821X/© 2021 The Author(s). Published by Elsevier B.V. This is an open access article under the CC BY-NC-ND license (http://creativecommons.org/licenses/by-nc-nd/4.0/).

mechanisms whereby the isotopic composition of continental margins is transmitted to ocean water remain unclear. As a result, this basic assumption still needs to be rigorously verified (Wilson et al., 2014).

"Boundary exchange" has been documented from changes in the concentration and isotopic composition of dissolved Nd in oceanic water masses that come into contact with continental margins, which indicate the addition of Nd from continents concurrent with the removal of Nd from seawater by particle scavenging (Lacan and Jeandel, 2005). However, the relative importance of several possible mechanisms for the addition of continental Nd to coastal waters has yet to be fully established. Continental Nd could be added to coastal water by run-off via rivers and groundwater, by partial dissolution of lithogenic particles discharged by rivers or released by coastal erosion, or by diffusion from pore waters after partial dissolution of lithogenic material in margin sediments (e.g. Abbott et al., 2015; Elderfield et al., 1990; Pearce et al., 2013; Rousseau et al., 2015). The relative importance of these different processes is likely site-specific.

The less radiogenic ε_{Nd} of the North Atlantic end member appears to be, in part, the result of unradiogenic Nd input from the Precambrian igneous and metamorphic rocks that dominate eastern Canada and Greenland, as the least radiogenic dissolved Nd measured in oceanic waters to date are found in Baffin Bay (Stordal and Wasserburg, 1986). In addition to receiving direct continental inputs from Greenland and Baffin Island, Baffin Bay also receives continental Nd from the Canadian Arctic Archipelago (CAA). The CAA forms a network of channels between a number of Arctic islands and the bordering mainland (Fig. 1), through which Pacific water flowing from the Canada Basin is chemically modified by contact with its extensive shoreline and relatively shallow (<650 m) seabed (Colombo et al., 2020; Michel et al., 2015). The rivers draining into the CAA from numerous islands and the northern continental margin represent a drainage area and water flow comparable to that of the largest North American Arctic river watersheds (Alkire et al., 2017; Holmes et al., 2012). Since their discharge occurs into geographically confined marine channels, they may have a particularly important impact on the ε_{Nd} of CAA water reaching Baffin Bay.

There has been a recent surge of interest in the geochemistry of small Arctic rivers, in particular in those draining into the marine straits of the CAA (Alkire et al., 2017; Brown et al., 2020; Colombo et al., 2019; Lafrenière and Lamoureux, 2008; Lewis et al., 2012; Li Yung Lung et al., 2018). These studies have demonstrated a large variability in the dissolved concentration and elemental composition of small CAA rivers. They have related trends in river dissolved load to the bedrock geology of the drainage basins and to latitudinal gradients in environmental conditions that control vegetation, permafrost, and dissolved organic matter concentrations. It is thus expected that similar variability will also be reflected in dissolved Rare Earth Elements (REE) concentration and Nd isotopic composition. As Arctic warming continues, runoff from land is predicted to transition from being surface dominated to groundwater dominated, likely resulting in a substantial increase in the discharge of dissolved constituents to the Arctic Ocean (Connolly et al., 2020; Frey and McClelland, 2009). Thus, considering that the dissolved load of Arctic rivers can be climate-sensitive, demonstrating that the small rivers draining the CAA may be significant contributors to the Nd signature of seawater transiting through the archipelago could bring into question whether the ε_{Nd} tagging of North Atlantic water is constant through time, with implications for the interpretation of the ε_{Nd} paleoceanographic records. As a first step towards assessing the importance of Arctic rivers in determining the ε_{Nd} of seawater flowing through the CAA, we report the <0.45 µm-filtrate REE concentration and ε_{Nd} (i.e., the concentration and ε_{Nd} of truly dissolved, nano-particulate and colloidal REEs passing through a 0.45 µm filter, hereafter referred to as dissolved) of thirteen rivers with different watershed lithology and draining into its major central and southern flow-paths through Parry Channel, Peel Sound, and Queen Maud Gulf (Table 1; Fig. 1). We then scale river inputs to the entire CAA to assess the importance of dissolved Nd discharged by rivers in determining the ε_{Nd} of seawater transiting from the Canada Basin to Baffin Bay.

2. Methods: sampling and analytical procedure

Thirteen rivers (Table 1) were accessed by helicopter from the CCGS *Amundsen* in August 2015 during the Canadian Arctic GEOTRACES cruise GN02 (Brown et al., 2020). Approximately five liter samples were collected manually by immersing 10-L acid-cleaned LDPE cubitainers below the surface and away from the banks of the rivers, while facing upstream. The samples were brought back on board and immediately filtered through single-use 0.45 µm pore size filter cartridges (AquaPrep®) before acidification to pH 2 with 6 N HCl. Most samples required two cartridges to complete the filtration, only one for rivers #7 and #9, and up to 10 cartridges for rivers with higher particle load (#2, #13, and #14). Aliquots (500 mL) were set aside for the measurement of REE concentration, and the remaining volume was processed for Nd isotopic measurements as described below. We note that the <0.45 µm-filtrate includes different fractions of REEs, i.e., truly dissolved, nano-particulate and colloidal fractions. As such, the <0.45 µm-filtrate is referred to as dissolved hereafter.

Nd isotopic composition analysis: Neodymium was co-precipitated from the remaining acidified sample by adding 50 to 100 mg of $FeCl_3$ and raising the pH to 8 with concentrated NH_4OH. After 36 to 48 h settling, the supernatant was drained and the precipitate was centrifuged for transport to the land-based laboratories (University of British Columbia, Vancouver, Canada; Laboratoire d'Etudes en Géophysique et Océanographie Spatiales - LEGOS, Toulouse, France). Fe precipitates were rinsed, dissolved in 6N HCl and passed through anionic columns (AG1-X8 100-200 mesh resin) for Fe separation in the French land-based lab. After this separation, a small fraction corresponding to ~500 mL of the initial sample volume was taken for a preliminary measurement of the REE concentrations on a high resolution (sector field) Inductively Coupled Plasma Mass Spectrometer (ICP-MS; Thermo Scientific Element XRTM), to estimate the quantity of REE spikes to add for the concentration determination by isotopic dilution (see the next paragraph) and the quantity of Nd for the isotopic measurement. From there, samples were processed as described in Grenier et al. (2013) for Nd separation and purification (through a cation exchange column packed with AG50W-X8 200-400 mesh resin and an anion exchange column packed with Ln-Spec resin), and were analyzed by thermal ionization mass spectrometry (TIMS) as described in Grenier et al. (2019).

REE analysis: REE concentrations were determined following the SeaSLOW method described in Pham (2020), at the French lab LEGOS. This method is based on an off-line pre-concentration system developed by Hatje et al. (2014). Briefly, pre-weighted sample aliquots (80-120 g) spiked in Nd, Eu, and Yb (aliquot mass and spike volume determined from the preliminary measurement mentioned above) were loaded onto ion-exchange columns packed with NOBIAS-chelate PA-1® resin that pre-concentrates REEs (SeaSLOW manifold). After several steps of separation and purification, REEs were eluted; this fraction was evaporated and then redissolved into 0.32 N HNO_3 for the measurement of REE concentrations on the ICP-MS Thermo Scientific Element XRTM by the external standard method, while Nd, Eu and Yb were additionally determined by isotopic dilution (recoveries >90% for all REEs; blanks <4 pg for La, Ce and Nd and <0.4 pg for all other REEs;

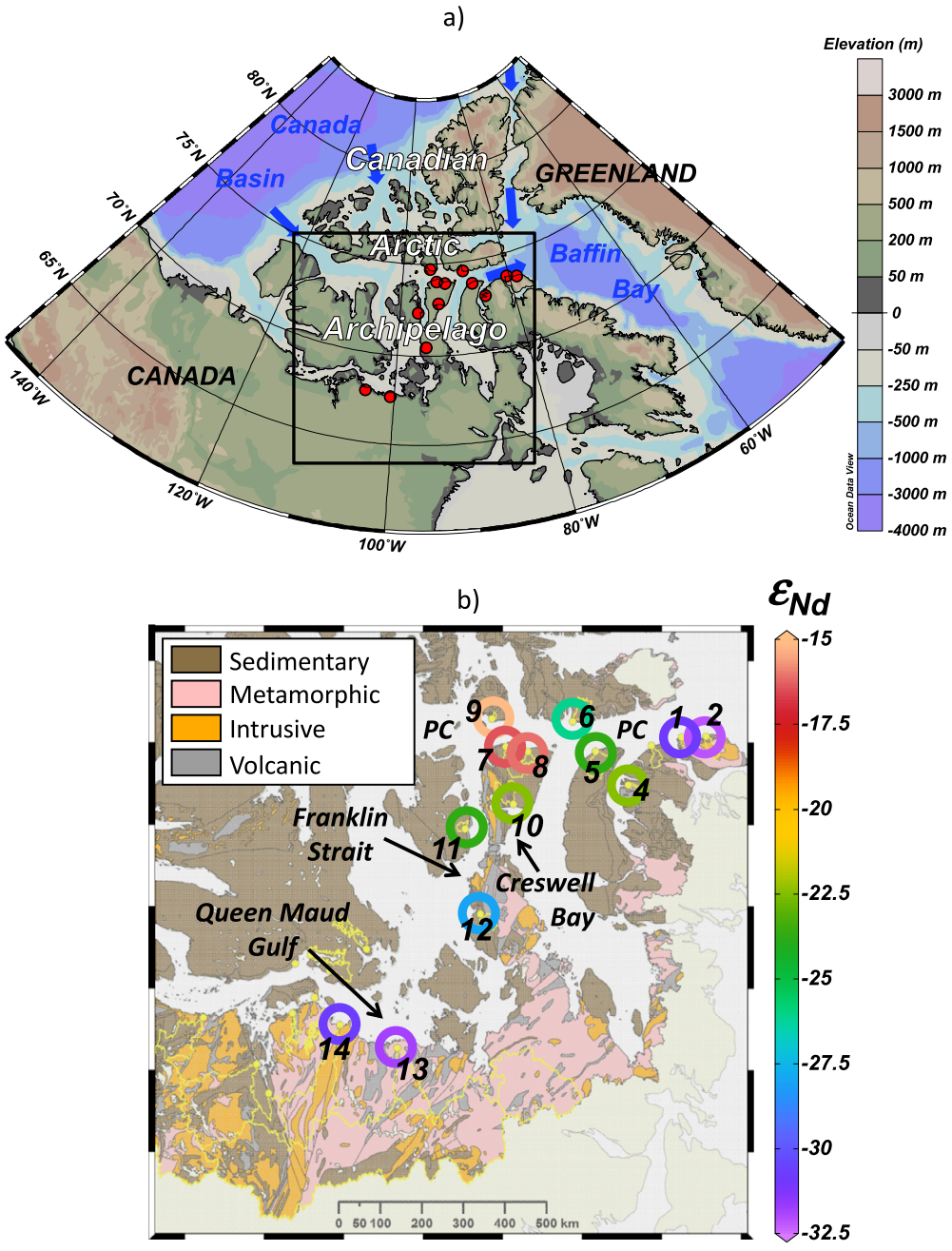

Fig. 1. a) Location of the study area, i.e. the northern coastal Canadian mainland and southeastern Canadian Arctic Archipelago (CAA). River sampling sites are identified with red dots. Elevation (in m) is given in color, and CAA inflows and outflows are shown by blue arrows. The black square delimits the geographic zone shown in b). b) Sampling locations are shown by circles with colors representing the dissolved neodymium isotopic composition of river water (expressed as ε_{Nd}, numbered following "River #" in Tables 1 and 2). The outline of the drainage basins (yellow lines) are superimposed on the dominant bedrock geology of the region, extracted from Brown et al. (2020), after Garrity and Soller (2009). PC: Parry Channel. (For interpretation of the colors in the figure(s), the reader is referred to the web version of this article.)

SLRS-6 validation). A desolvating nebulizer (Aridus II) was coupled to the ICPMS to prevent oxide interferences (Ce oxide rate: 0.06%).

pH: River water pH was determined from dissolved inorganic carbon (DIC), total alkalinity (TA), salinity, and *in situ* temperature (Brown et al., 2020; Table 1). DIC and TA were measured at T = 25°C and the river pH was calculated using the average measured *in situ* river temperature for the central CAA (Rivers #1-10, T = 3.93°C) and southern CAA (Rivers #11-14, T = 8.98°C). pH was calculated using the MS Excel macro spreadsheet CO2SYS v2.1 developed by Pierrot et al. (2006), using the stoichiometric equilibrium constants derived for freshwater by Millero (1979). For the calculation of freshwater pH, only [HCO_3^-], [CO_3^-], [OH^-], and [H^+] are included in the definition of TA and calculated pH is given without a reference to a particular pH scale (see Pierrot et al., 2006, for more details).

Ionic strength: The ionic strength of river water (I) was calculated from the molar concentration of the major ions (HCO_3^-, CO_3^-, Cl^-, SO_4^{2-}, Ca^{2+}, Mg^{2+}, Na^+, and K^+; Brown et al., 2020) using the following equation:

$$I = \frac{1}{2}\sum_i C_i \cdot Z_i^2$$

where C_i and Z_i are the molar concentration and charge of each ion (Table 1).

Table 1
Name, sampling location, drainage basin characteristics, pH and ionic strength of the thirteen CAA rivers reported in this study (sampled between August 11 and 18 2015; from Brown et al., 2020). I. = Intrusive; M. = Metamorphic; S. = Sedimentary; V. = Volcanic. These rivers were sampled for analyses of dissolved and particulate trace metals (Colombo et al., 2019) and major dissolved constituents (Brown et al., 2020). Numbers and river names follow those reported in these studies. River #3 (Charles York River; Brown et al., 2020) was not sampled for REEs and trace metals.

River #	Name	Lat (°N)	Lon (°E)	Drainage Basin Area (km^2)	Bedrock Geology				% Glacier Ice	pH[a]	Ionic Strength[b] (mmol/L)
					% I.	% M.	% S.	% V.			
#1	Akpat Kuunga*	73.8	−80.4	96	0	13	87	0	46	8.0	1.54
#2	Glacier River*	73.6	−78.7	983	44	38	17	1	83	8.1	0.39
#4	Marcil Creek	73.0	−85.0	128	0	0	100	0	0	7.5	0.56
#5	Saaqu River	73.8	−81.0	2220	0	0	100	0	0	8.7	2.91
#6	Devon Island*	74.5	−88.5	1310	0	0	100	0	8	8.7	2.08
#7	Cunningham River	74.0	−93.6	2155	0	0	100	0	0	8.7	3.58
#8	Garnier River	73.9	−92.0	480	0	0	100	0	0	8.7	4.60
#9	Mecham River	74.7	−94.8	104	0	0	100	0	0	8.5	4.27
#10	Creswell River	72.8	−93.4	1773	27	0	73	0	0	8.6	4.90
#11	Le Feuvre Inlet*	72.3	−96.9	357	0	0	100	0	0	8.7	5.31
#12	Pasley River	70.5	−95.6	1214	0	0	100	0	0	8.7	3.30
#13	Simpson River	67.7	−100.6	7082	7	69	24	0	0	7.1	1.90
#14	Ellice River	67.9	−104.1	16938	53	45	1	1	0	7.0	0.80[c]

* Named according to distinctive features of the region, following Colombo et al. (2019) and Brown et al. (2020), due to the lack of official name on available charts.
[a] pH was determined following Pierrot et al. (2006) using the stoichiometric equilibrium constants (K1, K2) derived for freshwater by Millero (1979) and is reported without a reference to a particular pH scale. The average error determined on pH calculations is ± 0.1.
[b] Ionic strength determined from major ion and inorganic carbon data reported in Brown et al. (2020).
[c] The ionic strength value for the Ellice River is reported for date of August 18th, 2015 when Nd samples were also collected, instead of using the averaged values reported in Brown et al., 2020.

CAA river flux determination (*scaling*): We used measured river Nd concentration values (estimated to be representative of ∼40% of the average annual Nd concentration, from Chupakov et al., 2020) to estimate an average annual riverine dissolved Nd flux for the entire CAA following the "end-member" (EM) scaling method outlined in Brown et al. (2020). For this study we applied the scaling approach using two EMs based on our sampled rivers: a sedimentary EM (drainage basin-weighted average of rivers #5, #6, #7, #8, #9, #11, #12; Table 1) and a combined intrusive-metamorphic-volcanic EM (River #14; Table 1). Further details can be found in the Supplementary Methods of Appendix A.

CAA marine flux determination: We used the Nucleus for European Modeling of the Ocean (NEMO) numerical framework, version 3.4, and the Arctic Northern Hemisphere Atlantic (ANHA) configuration, run at 1/12 degree, to determine the volume flux through the CAA, as summarized in Grivault et al. (2018) and detailed in the Supplementary Methods of Appendix A. For this study, we resampled and extended the Grivault et al. (2018) analysis to cover the period of observations (2013-2018) and closed the budget to estimate the total volume transport through the region by including the narrow channels connecting into Parry Channel and out of Lancaster Sound. Further details can be found in the Supplementary Methods of Appendix A.

3. Results

3.1. Nd isotopic compositions (ε_{Nd}) and concentrations

The dissolved ε_{Nd} of CAA rivers was highly variable (−32.1 to −15.1; Table 2; Fig. 1) and generally much less radiogenic (i.e. more negative) than the dissolved Nd found in the larger Arctic rivers ($\varepsilon_{Nd} = -14.2$ to -5.2; Table A1). The rivers with the least radiogenic composition (i.e. most negative ε_{Nd}; rivers #1, #2, #13 and #14; $\varepsilon_{Nd} = -32.1$ to -30.7) tended to have high proportions of Precambrian intrusive and metamorphic rocks in their drainage basins (#1: 13%; #2: 82%; #13: 76%; #14: 98%; Table 1). These formations are found on Bylot Island (#1 & #2) and the northern continental margin of Nunavut (#13 & #14; Fig. 1). On the other hand, the rivers #7, #8 and #9 had the most radiogenic Nd composition (i.e. least negative; $\varepsilon_{Nd} = [-16.1; -15.1]$), and drained exclusively younger sedimentary rocks (Ordovician-Silurian; see Fig. 1 of Colombo et al., 2019) on Cornwallis and northern Somerset islands. The remaining six rivers with intermediate Nd isotopic composition (#4, #5, #6, #10, #11 and #12; $\varepsilon_{Nd} = [-28.0; -22.4]$) also drained sedimentary rocks (although older –Middle Proterozoic– for river #4), except for river #10 ($\varepsilon_{Nd} = -22.4$) that had 27% of its drainage basin covered by Precambrian intrusive rocks (Table 1).

The range of dissolved Nd concentration measured in the CAA rivers is very large (8–37,260 pmol/kg; Table 2) and encompasses the range measured in the largest Arctic rivers (111–2,152 pmol/kg; Table A1). The rivers with Precambrian intrusive and metamorphic rocks in their drainage basins and with very unradiogenic dissolved Nd (#1, #2, #13, and #14) have much higher dissolved Nd concentrations (1,433–37,260 pmol/kg) than rivers with drainage basins composed entirely of sedimentary rocks (8–488 pmol/kg). However, there is no correlation between ε_{Nd} and [Nd] within these two subgroups (Fig. 2). Rivers #2 and #4 stand out, with Nd concentration of river #2 more than ten-fold higher than the other rivers with similar bedrock geology, and Nd concentration of river #4 more than ten-fold higher than the average concentration in all other rivers draining exclusively sedimentary bedrock.

3.2. PAAS-normalized REE patterns

Normalization of REE concentrations to a reference eliminates the large even-odd variation in natural REE abundance (the Oddo-Harkins effect) to better visualize their environmental fractionation. Here we normalize to Post Archean Australian Shale (PAAS; McLennan, 2001), a commonly used reference representative of the REEs of the upper continental crust. This normalization reveals environmental fractionation between the light (LREEs), middle (MREEs) and heavy REEs (HREEs). It can also reveal anomalies, i.e. fractionation of one REE compared to its neighbors, as

Table 2
Neodymium isotopic compositions (expressed as ε_{Nd}, with associated standard error 2σ) and REE concentrations measured in the CAA river samples of this study (i.e., from the dissolved and colloidal REEs passing through a 0.45 μm filter).

River #	ϵ_{Nd}	2σ	La	Ce	Pr	Nd	Sm	Eu	Gd (pmol/kg)*	Tb	Dy	Ho	Er	Tm	Yb	Lu
#1	−30.8	0.1	1445.54	3228.23	377.63	1433.31	237.47	40.79	140.31	23.91	126.85	21.86	57.19	7.32	39.91	6.12
#2	−32.1	0.1	31095.31	79444.99	9375.49	37260.41	6004.28	1092.16	3258.54	475.76	2240.17	376.88	980.77	123.10	690.68	104.92
#4	−22.4	0.1	304.76	626.29	104.83	488.40	120.22	25.86	87.98	15.97	85.40	15.51	40.68	5.58	33.00	4.77
#5	−23.6	0.1	9.84	18.62	2.49	10.61	1.97	0.36	1.43	0.27	1.72	0.38	1.19	0.18	1.02	0.18
#6	−26.0	0.1	35.65	86.11	10.01	39.82	6.65	1.18	4.18	0.78	4.82	1.01	3.02	0.44	2.65	0.41
#7	−16.1	0.3	5.35	4.62	1.49	8.09	1.85	0.38	1.68	0.33	2.41	0.60	2.06	0.32	2.13	0.36
#8	−16.0	0.1	27.69	78.84	10.30	44.85	9.04	1.68	6.05	1.21	7.94	1.66	4.93	0.73	4.59	0.60
#9	−15.1	0.2	26.93	16.29	6.00	27.45	5.15	1.07	4.73	1.04	7.66	1.82	5.78	0.82	5.07	0.76
#10	−22.4	0.4	24.87	31.15	5.48	24.89	4.69	0.94	3.74	0.74	5.04	1.16	3.64	0.53	3.24	0.53
#11	−23.6	0.1	61.36	50.42	14.73	67.35	12.75	3.18	10.09	2.01	13.63	3.07	9.44	1.33	8.26	1.32
#12	−28.0	0.1	71.05	45.27	15.93	71.48	12.15	1.94	8.71	1.47	8.69	1.85	5.42	0.74	4.57	0.71
#13	−31.7	0.1	1750.78	3449.94	416.11	1617.51	249.90	40.81	150.22	22.39	114.33	21.04	57.26	7.93	46.22	7.39
#14	−30.7	0.1	2360.13	4043.63	550.05	2120.87	327.49	53.20	196.84	30.21	156.42	29.45	80.84	11.20	68.05	10.46

* average precision (2σ) ranged from 2 to 5% for Y, 2 to 6% for Gd, 1 to 3% for Lu and 1 to 2% for the remaining REEs.

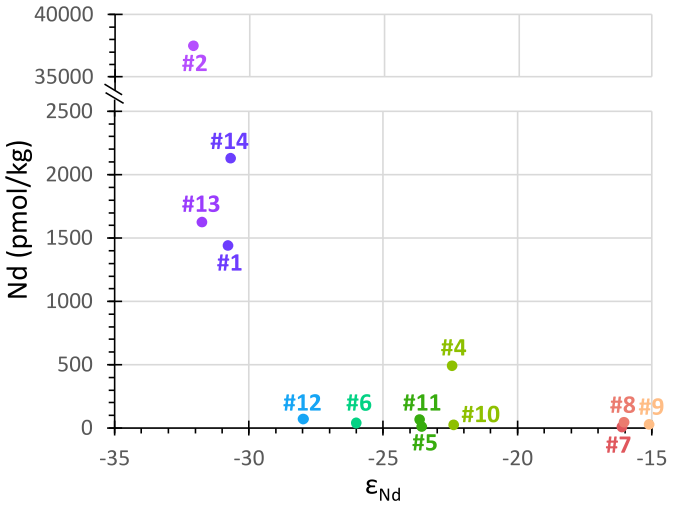

Fig. 2. Dissolved [Nd] versus ε_{Nd} measured in the thirteen CAA rivers sampled in this study. Dots are colored following ε_{Nd} in Fig. 1. River #2 has much higher [Nd] than the other rivers with intrusive and/or metamorphic rocks in their drainage basins (#1, #10, #13, #14), while river # 4 has much higher [Nd] than the other rivers with drainage basins consisting exclusively of sedimentary rocks (#5, #6, #7, #8, #9, #11, #12).

commonly observed for Ce due to the low solubility of the oxidized form of this element (Ce^{4+}; the Ce anomaly is defined as $Ce/Ce^* = [Ce]_n/(2^*[Pr]_n - [Nd]_n$, where [X]n is the concentration of element X normalized to its concentration in PAAS; Bolhar et al., 2004). A Ce anomaly <1 (called a "negative" anomaly) indicates of deficit of Ce compared to the other LREEs, which occurs in oxic waters as a result of the oxidation of Ce(III) to Ce(IV) and its subsequent preferential removal from the dissolved phase by adsorption onto metal (hydr-)oxides (Elderfield, 1988).

PAAS-normalized REE patterns also subdivide the CAA rivers into the same two broad groups as Nd concentrations and isotopic composition (Fig. 3): a) those enriched in the LREEs (La-Eu) including rivers #1, #2, #13 and #14, which are the rivers with the least radiogenic ε_{Nd} and the highest dissolved Nd concentrations; b) those slightly to significantly enriched in HREEs (Gd-Lu), which correspond to rivers with more radiogenic ε_{Nd} and lower dissolved Nd concentrations (rivers #5 to #12), which only drain sedimentary rocks (with the exception of river #10; Table 1). Among those, rivers #5, #6, and #8 have no measurable or a very modest negative Ce anomaly while rivers #7, #9, #10, #11, and #12 show a more prominent negative Ce anomaly (Table 3). Again, river #4 stands out with higher concentrations of MREEs (Sm-Dy) compared to heavier and especially to lighter REEs. Similar patterns have been observed in other Arctic rivers (Fig. A1). Rivers from southwestern Greenland (Tepe and Bau, 2015) and southeastern Hudson Bay (Goldstein and Jacobsen, 1988) are LREE enriched, similar to CAA rivers #1, #2, #13 and #14, while HREE enriched rivers, characterized by a more pronounced negative Ce anomaly, have been found in Northern Sweden (Ingri et al., 2000). Rivers displaying a MREE-enrichment, such as river #4, have been observed in Central Alaska (Stolpe et al., 2013).

4. Discussion

4.1. Factors controlling the dissolved REE concentration and Nd isotopic composition of CAA rivers

The thirteen CAA rivers analyzed in this study can generally be subdivided into two categories that broadly reflect the bedrock geology of their watersheds. The lithology of the CAA generally shows a transition from younger sedimentary rocks (Devonian) on the western end, to older sedimentary (Silurian, Ordovician, Proterozoic) and igneous or metamorphic (Proterozoic or Archean) rocks to the east (Okulitch, 1991). From the geological database Earthchem (http://www.earthchem.org), rocks that exhibit the most LREE-enriched patterns and least radiogenic ε_{Nd} in the CAA are Precambrian metamorphic gneiss and igneous carbonatite ($\varepsilon_{Nd} = [(-31.6) - (-29.6)]$; Mackie et al., 2009; Villeneuve and Relf, 1998). Four rivers (#1, #2, #13 and #14) have higher dissolved Nd concentrations, with a less radiogenic isotopic composition (Fig. 2) and PAAS-normalized REE patterns with a LREE enrichment (Fig. 3a). These four rivers all drain bedrock partly made of metamorphic rocks, although in different proportions (13-69%; Table 1). The remaining nine rivers have lower dissolved Nd concentrations, with a more radiogenic isotopic composition (Fig. 2) and PAAS-normalized REE patterns showing a heavy REE enrichment, with or without a negative Ce anomaly (Fig. 3b-c). These nine rivers have drainage basins consisting of sedimentary rocks from the Paleozoic (or from the Proterozoic for river #4; see Fig. 1 of Colombo et al., 2019), except river #10, which also drains some intrusive rock (Table 1). This broad subdivision clearly shows the importance of bedrock geology in determining the concentration and isotopic composition of dissolved Nd, and the PAAS-normalized pattern of REEs, as has also been noted for the concentrations of other dissolved elements (Alkire et al., 2017; Brown et al., 2020; Colombo et al., 2019).

Another factor affecting the Nd concentration of rivers is the presence of ice sheets in their drainage basins. Only two of the thirteen rivers sampled have a large fraction of their watershed covered by an ice sheet (#1: 46%; #2: 83%; Table 1). Both these rivers have high but very different dissolved Nd concentrations (#1: 1,433 pmol/kg; #2: 37,260 pmol/kg; Fig. 2). In addition to having a larger ice sheet in its drainage basin, river #2 also has a much higher proportion of intrusive and metamorphic bedrock (#1: 13% and 0% of metamorphic and intrusive rocks, respectively; #2: 38% and 44% of metamorphic and intrusive rocks, respectively; Table 1). The contrast between river #1 and #2 thus suggests that the presence of crystalline bedrock and extent of glacial cover over the drainage basin, both of which are significantly higher for river #2, exert primary controls on Nd concentration in CAA rivers. With its smaller glaciated area and smaller drainage area consisting of metamorphic rocks, river #1 has lower dissolved Nd concentration, but its unradiogenic ε_{Nd} (Fig. 2) suggests that much of this dissolved Nd comes from Precambrian crystalline rocks. River #6

Table 3
Ce anomaly ($Ce/Ce^* = [Ce]_n/(2^*[Pr]_n - [Nd]_n$) and PAAS-normalized REE pattern slope (expressed as $[Yb]_n/[Nd]_n{}^*10^6$). $[X]_n$ is the concentration of element X normalized to its concentration in PAAS (McLennan, 2001).

River #	Ce/Ce^*	$[Yb]_n/[Nd]_n$
#1	0.95	0.39
#2	0.99	0.26
#4	0.87	0.96
#5	0.95	1.37
#6	1.01	0.94
#7	0.62	3.73
#8	1.00	1.45
#9	0.38	2.62
#10	0.79	1.85
#11	0.48	1.74
#12	0.39	0.91
#13	0.94	0.40
#14	0.83	0.46

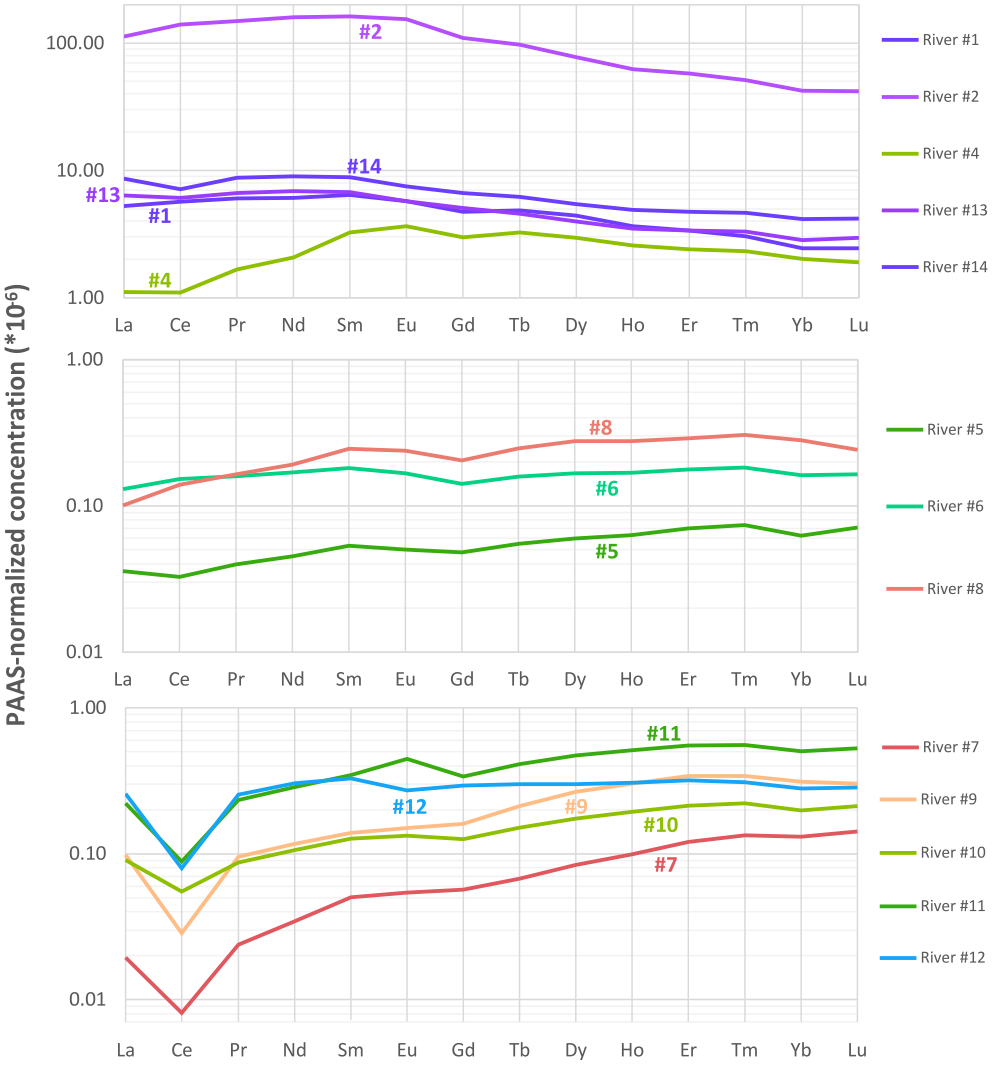

Fig. 3. PAAS-normalized REE patterns in the CAA rivers, colored following ε_{Nd} in Fig. 1, showing (a) light REE (rivers #1, #2, #13, #14) and middle REE (river #4) enrichment; (b) heavy REE enrichment with no or modest negative Ce anomaly (rivers #5, #6 and #8); (c) heavy REE enrichment with a more prominent negative Ce anomaly (rivers #7 and #9 to #12).

(Devon Island) also has a small glaciated area in its drainage basin (8%; Table 1), but its watershed consists exclusively of sedimentary rocks, which results in low dissolved Nd concentration and a more radiogenic isotopic composition ($\varepsilon_{Nd} = -26$). On the other hand, notwithstanding the lack of glaciated areas in their drainage basins, river #13 and #14 have comparatively high dissolved Nd concentrations and unradiogenic ε_{Nd} due to the dominance of intrusive and metamorphic rocks in their drainage basins (76% and 98%, respectively). These two rivers also have the highest dissolved organic carbon (DOC) concentrations (Fig. 4a; Brown et al., 2020), which help maintain –through complexation with organic and organo-mineral colloids– high concentration of colloidal REEs, Fe and Al (Pokrovsky et al., 2010; Pokrovsky and Schott, 2002). The latter two elements were also found in relatively high concentrations in these two rivers, although for a lower filtration cutoff (<0.2 µm-filtrate; Colombo et al., 2019).

There are two rivers that do not fit this general pattern. River #4 has a very small drainage basin on the northern tip of Baffin Island with an unglaciated watershed consisting entirely of sedimentary rocks. Yet, its dissolved Nd concentration is about 10 times higher than in the other CAA rivers draining a 100% sedimentary bedrock geology (Fig. 2). River #4 also stands out as the only one showing MREE enrichment (Fig. 3a), and having Proterozoic sedimentary rocks dominating its watershed (Colombo et al., 2019). On the other hand, river #10 has some intrusive rocks in its drainage basin (27%; Table 1) and yet has a dissolved Nd concentration as low as all the rivers draining exclusively sedimentary bedrock (Fig. 2).

Results from earlier studies have generally shown a similar range of dissolved Nd concentrations and PAAS-normalized patterns in river water, although never as high as in river #2. Goldstein and Jacobsen (1988) found high <0.2 µm-filtrate Nd concentration and LREE enrichment in a Canadian Shield draining river (eastern Hudson Bay) and in a lake from Western Greenland (1,158 and 3,134 pM, respectively). In contrast, the <0.2 µm-filtrate Nd concentrations in three large global rivers (Mississippi, Ohio, Indus) were lower (22 - 140 pM), as well as the <0.45 µm-filtrate Nd concentration of Amazon water (880 pM), with a HREE enrichment and varying Ce anomalies. Two rivers draining volcanic terrain also had low <0.2 µm-filtrate Nd concentration (60 and 345 pM) and HREE enrichment, but no Ce anomaly. Goldstein and Jacobsen (1988) also observed that, among the rivers they analyzed, the filtrates with the highest Nd concentration had the lowest pH. A similar trend is also observed in the CAA rivers. The

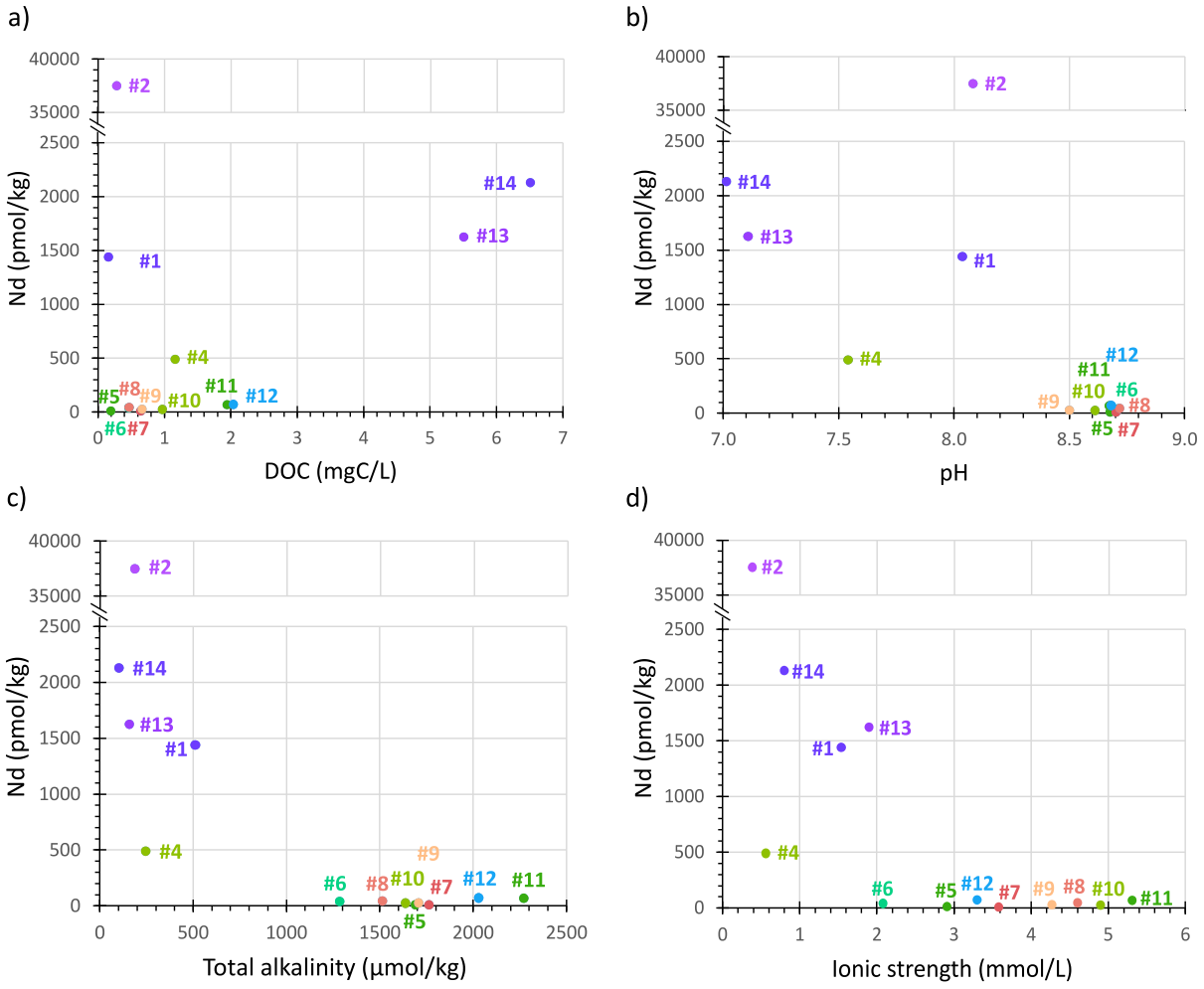

Fig. 4. (a) Variations in the dissolved Nd concentration in the CAA rivers as a function of (a) dissolved organic carbon (DOC, in mgC/L), (b) pH, (c) total alkalinity (TA, in µmol/kg), and (d) ionic strength (in mmol/L). DOC and TA are from Brown et al. (2020); pH and ionic strength (Table 1) were determined as described in the Methods section. All parameters were determined on <0.45 µm filtrates, except from DOC (<0.22 µm-filtrate). Dots are colored following ε_{Nd} in Fig. 1.

five rivers with the highest dissolved Nd concentration have lower pH (Fig. 4b). Low pH reduces adsorption of ionic REEs on particle surfaces and helps explain the relatively high dissolved Nd concentration in river #4 (pH = 7.5; Table 1) compared to the other rivers draining sedimentary rocks (pH = [8.5; 8.7]). It is unclear, however, why this river has a lower pH, notwithstanding the dominance of sedimentary rocks in its watershed. The dissolved MREE enrichment and relatively high concentrations of <0.2 µm-filtrate DOC and Fe (Colombo et al., 2019) suggest the presence of organic/iron-rich nanocolloids, as observed in <0.45 µm-filtrates of Alaskan rivers during the spring flood, from the erosion of organic-rich soil (Stolpe et al., 2013; Fig. A1). The low dissolved Nd concentration in river #10 is consistent with its higher pH, reflecting the dominance of carbonate weathering in its drainage basin.

Elderfield et al. (1990) indicated that the operationally defined dissolved fraction of REEs in river water consists of two pools: truly dissolved and colloidal. They found a clear dependency between the degree of HREE enrichment of the shale-normalized patterns and REE concentration, which is also recognized in the CAA rivers (Fig. 5). They attributed this trend to the dominance of colloids in rivers with high REE concentrations. In glacier-fed rivers, such as river #1 and #2, inorganic colloids could be produced by abrasion of the bedrock by the ice sheet (Tepe and Bau, 2016), and their REE patterns would remain the same as that of the bedrock (Tepe and Bau, 2015; Fig. A1). In the absence of ice sheets, as in river #13 and #14, congruent dissolution of rocks and subsequent formation of stable Fe-organic matter colloids could also produce organic colloids with the same REE pattern as the bedrock (Pokrovsky et al., 2010; Pokrovsky and Schott, 2002). Thus, dominance of colloidal Nd could explain the high dissolved Nd concentration observed in river #1, #2, #13 and #14, and their PAAS-normalized REE patterns showing light REE enrichment would reflect the bedrock of their watershed (as is also observed in <0.45 µm-filtrates of other boreal river waters; Ingri et al., 2000; Fig. A1). The latter is confirmed by the observation that the LREE enrichment found in high [Nd] rivers draining the Canadian and Greenland Shield disappears when <0.2 µm-filtrate REE concentrations are normalized to those measured in the suspended particles (Fig. 4 of Goldstein and Jacobsen, 1988), indicating that the REE pattern in these rock formations is LREE enriched when normalized to PAAS. If high Nd concentration reflects the presence of organic or inorganic colloidal Nd, we would also expect that [Nd] would depend on the ionic strength of river water or the DOC concentration. Indeed, river #13 and #14 have comparatively high DOC concentrations (Fig. 4a), which could stabilize colloidal Nd (along with Fe and Al; Colombo et al., 2019). On the other hand, river #1 and #2, while having low DOC concentrations (Fig. 4a), have among the lowest ionic strengths (Fig. 4d), which would keep colloids in suspension.

The order of magnitude difference in dissolved Nd concentration between river #2 and the other three rivers with high REE concentrations (#1, #13 and #14) was also observed for some

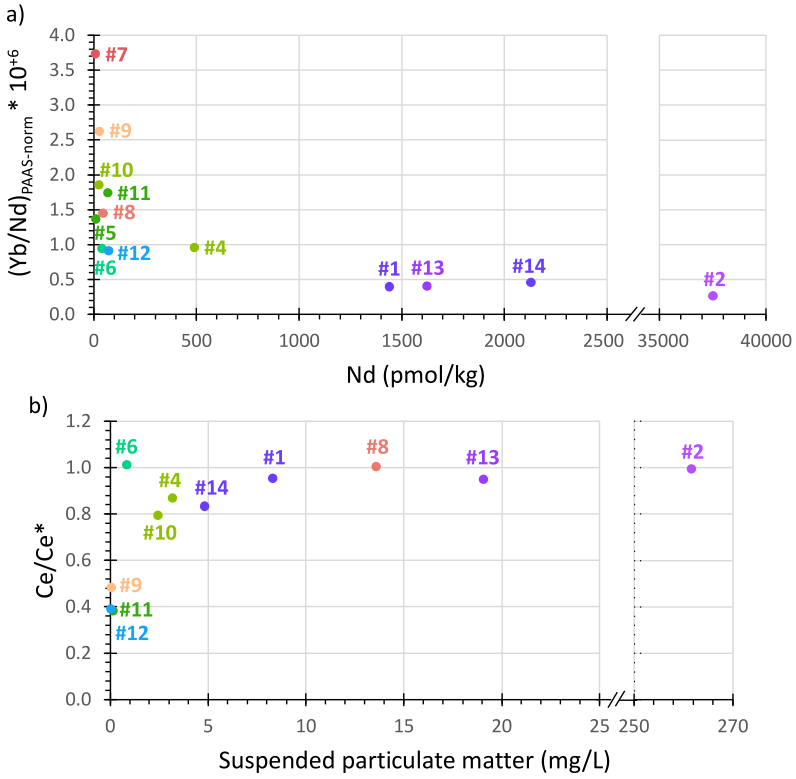

Fig. 5. a) PAAS-normalized REE pattern slope (expressed as $(Yb/Nd)_{PAAS\text{-}norm}*10^6$) of the CAA river waters –greater than 1 if enriched in HREEs– as a function of dissolved Nd concentration (in pmol/kg). b) Dissolved Ce anomaly (Ce/Ce^*) as a function of the concentration of suspended particulate matter (SPM; in mg/L). SPM concentrations are from Colombo et al. (2019; their Table S1) and represent the weight of material recovered on 0.22 µm filters per volume of water filtered, for TM analysis. Dots are colored following ε_{Nd} in Fig. 1.

trace metals and tentatively attributed to a high fraction of colloids included in the operational definition of the dissolved fraction (defined as <0.2 µm-filtrate for trace metals; Colombo et al., 2019). The dominance of colloids in the <0.2 µm-filtrate of this river is supported by its partition coefficient K_d (particulate over <0.2 µm-filtrate concentration ratio), which is lower for Mn and especially Ga compared to the other rivers (Colombo et al., 2019). A decrease in K_d with increasing suspended particle load has often been observed and attributed to the inclusion of an increasing proportion of colloidal particles in the dissolved phase (e.g., Benoit and Rozan, 1999; Tang et al., 2002). The dissolved Nd concentration in river #2 could thus consist mostly of colloids produced by the abrasive action of ice sheets on crystalline rocks, and stabilized in the low ionic strength water resulting from the limited chemical weathering occurring under these conditions. However, caution must be taken when comparing REE and trace metal concentrations of these rivers, as different filtration cut-offs were used (0.45 µm for REEs, 0.2 µm for trace metals). The order of magnitude difference of concentration between river #2 and rivers #1, #13 and 14 is not observed for Fe and Al (Colombo et al., 2019). If much of the colloidal REE, Fe and Al fraction in river #2 is in the 0.2-0.45 µm size range, this operational difference could provide an explanation.

In rivers #5 to #12, with lower Nd concentration, dissolved REEs could be subjected to fractionation - if mostly truly dissolved - by adsorption on particle surfaces, resulting in LREE depletion and thus relative HREE enrichment. Preferential scavenging of LREEs is expected to be more pronounced in rivers with higher carbonate alkalinity, as HREEs form stronger carbonate complexes that are less susceptible to removal by adsorption on particles (Byrne and Kim, 1990). In the CAA rivers, total alkalinity (TA) is essentially carbonate alkalinity (Brown et al., 2020) and the rivers with higher PAAS-normalized Yb/Nd ratios (i.e., rivers #5 to #12; Fig. 5; Table 3) also have higher TA (Fig. 4c). However, the PAAS-normalized Yb/Nd ratio for the CAA rivers with lower dissolved Nd concentration varies widely (Fig. 5). If environmental REE fractionation occurs within these river systems, we would expect to find a dependency between the PAAS-normalized Yb/Nd and TA. Since there is no such correlation, environmental REE fractionation within these river systems is unlikely to be the main controlling factor for their REE patterns. Instead, the HREE enrichment, and the Ce anomaly displayed by some of the rivers (Fig. 3), must be largely inherited from the carbonate rocks of their drainage basin, which have acquired their REE pattern, Ce anomaly and ε_{Nd} from ancient seawater. Such patterns have been attributed to the dominance of truly dissolved inorganic REEs, associated with carbonate ligands (Pourret and Tuduri, 2017; Rousseau et al., 2015). The inherited negative Ce anomaly also seems to be sensitive to the concentration of suspended particulate matter (SPM; SPM concentrations are from Colombo et al., 2019, reported in their Table S1) and appears to diminish in most rivers within the SPM concentration range of [0-5] mg/L (Fig. 5b). As colloid concentrations increase with SPM concentrations (Benoit and Rozan, 1999), the disappearance of the Ce anomaly with increasing SPM concentration must reflect the increasing dominance of colloids in the dissolved Nd concentrations. Goldstein and Jacobsen (1988) reported a relationship of the Ce anomaly with pH that we do not observed in our data, but this might be due to the greater colloidal fraction included in the samples of our study compared to theirs (they used a filter pore size of 0.2 µm where we used 0.45 µm).

In summary, the concentration of dissolved Nd (and all REEs to a different extent) of CAA rivers increases when drainage basin lithology is dominated by metamorphic bedrock and is overlain by ice sheets. Under these conditions, dissolved Nd is likely mostly colloidal and the REE pattern reflects that of the bedrock underlying the drainage basin. Metamorphic rocks have relatively high

Nd concentration (average [Nd] in gneiss = $2.29\,10^6 \pm 1.81\,10^6$ pmol/kg; n = 2498; database www.earthchem.org/) compared to carbonate rocks ($3.26\ 10^5$ pmol/kg; Veizer, 1983), which could, in part, explain the difference in Nd concentration between the two groups of CAA rivers. In addition, colloids are destabilized with increasing ionic strength. The very high dissolved REE concentrations in river #2, associated with a very high concentration of SPM, is consistent with earlier suggestions that high REE concentrations are not truly dissolved but rather mostly colloidal (Elderfield et al., 1990). The very low ionic strength of this river (Fig. 4d) reflects limited chemical weathering in the drainage system, dominated by metamorphic rocks and ice covered areas (Table 1); this low ionic strength allows for higher concentrations of colloidal Nd (Fig. 2). River #1 has similarly low ionic strength, but the smaller area of its watershed consisting of crystalline bedrock under ice likely results in a much lower (albeit still relatively high) colloidal Nd concentration. The other two rivers with high Nd concentrations (#13 and #14) also have relatively low ionic strength and relatively high DOC (Fig. 4a), Fe and Al (Colombo et al., 2019), which may contribute to relatively high colloidal REE concentrations produced by dissolution of minerals with relatively high REE concentrations. On the other hand, the rivers with low Nd concentrations have a wide range of ionic strength (Fig. 4d), low DOC (Fig. 4a) and higher pH (Fig. 4b). However, the lack of correlation between Nd concentration and ionic strength, pH or DOC indicates that colloid stability or adsorption on particle surfaces do not play a major role in determining Nd concentration and REE pattern in these rivers. Therefore, their low Nd concentrations and PAAS-normalized REE patterns must reflect the low concentration and the seawater-like REE pattern of the sedimentary rocks within their watersheds.

4.2. The importance of CAA rivers in altering the ε_{Nd} of Pacific water transiting through the CAA

As outlined in the introduction, it is important to understand the factors controlling the relatively unradiogenic Nd isotopic composition found in the North Atlantic. The CAA is the main pathway through which radiogenic Pacific Water reaches the North Atlantic, and as such, alteration of the Nd isotopic composition of this water mass towards less radiogenic values during its transit through the CAA has potentially important implications for the control of ε_{Nd} in the North Atlantic. The relatively more radiogenic seawater entering the CAA ($\varepsilon_{Nd} = [-5.8; -10.3]$, see station CB2 in Grenier et al., 2019) becomes increasingly less radiogenic as it travels towards Baffin Bay (I. Baconnais, pers. commun., 2020). To assess whether CAA rivers contribute significantly to altering the Nd isotopic composition of this water mass, we estimate the discharge rate of dissolved Nd by rivers into the CAA relative to the flow of dissolved Nd in seawater transiting from the Canada Basin to Baffin Bay.

Following an "end-member" (EM) scaling approach (see Supp. Methods of Appendix A), we estimate an average riverine dissolved Nd flux for the entire CAA by scaling the dissolved Nd concentration measured in rivers draining two EM rock types that make up the CAA drainage area: sedimentary bedrock and intrusive-metamorphic-volcanic bedrock. Although we lack information on seasonal changes in the dissolved Nd concentration of CAA rivers, a recent study has shown that dissolved REE concentrations in high Arctic rivers are higher during spring melting, and concentrations measured in late summer are about 40% of the annual average concentration (Table S1 of Chupakov et al., 2020). Considering that our river sampling was conducted in late summer (August), if this seasonality holds for the thirteen CAA rivers we sampled, scaling Nd concentrations from rivers draining the two end members (sedimentary bedrock and intrusive-metamorphic-volcanic bedrock) to their proportional coverage across the CAA yields a riverine dissolved Nd flux for the entire CAA of 0.4×10^6 mol/yr (see Supp. Methods of Appendix A).

To estimate the marine dissolved Nd flux, we determine the annual mean transport of seawater through the CAA over 2013-2018, following Grivault et al. (2018; see Supp. Methods of Appendix A). This yields an annual transport of 0.65 Sv through the south-central CAA marine system. Taking the Nd concentration measured at the western end of Parry Channel as representing the Nd concentration of water entering the CAA from the Canada Basin (21 ± 3 pmol/kg; I. Baconnais, pers. commun., 2020) provides an estimate of the marine dissolved Nd flux entering the CAA of 0.44×10^6 mol/yr.

Thus, we estimate a flow of dissolved Nd transported by Arctic rivers discharging into the CAA equivalent to the Nd flux of seawater entering the CAA. A large fraction of dissolved Nd discharged by rivers is typically removed from solution during estuarine mixing; it has been shown to vary from 40% to 90% in the fifteen different estuaries reported in Rousseau et al. (2015; $71\% \pm 16\%$ on average). Therefore, the impact of river water on the Nd of seawater exiting the CAA will be dictated by the percentage of Nd removal during mixing with seawater; it could be modest (if 90% removal) or more significant (if $\ll$90% removal). Further constraining the actual contribution of rivers to seawater ε_{Nd} exiting the CAA requires quantification of Nd removal in Arctic river estuaries or mass and isotopic balance calculation in the CAA. Thus, notwithstanding the uncertainties in these calculations, if the dissolved Nd concentration of CAA rivers increases significantly as a result of warming (Connolly et al., 2020; Frey and McClelland, 2009), this could imprint a climate sensitive ε_{Nd} to the CAA water entering Baffin Bay, as evidenced on glacial-interglacial timescales by the Northern Atlantic Nd isotope end member variability (Zhao et al., 2019). The northern ε_{Nd} shift (about 1 ε-unit lower) was attributed to input of poorly weathered material, originating from Greenland and North America, after the ice sheets retreated late in the deglaciation, which released substantial amounts of unradiogenic Nd (Howe et al., 2016; Pöppelmeier et al., 2020).

5. Conclusion

The <0.45 µm-filtrate REE concentration of CAA rivers is dominantly controlled by drainage basin lithology and the presence of ice sheets within the watershed, while their ε_{Nd} and PAAS-normalized REE pattern reflects that of the bedrock in their drainage basin. The abrasive action of glaciers on crystalline rocks appears to be a particularly efficient mechanism to increase the colloidal load of REEs in glacier-fed rivers and their discharge in coastal waters.

We calculate that the flow of dissolved Nd transported by Arctic rivers discharging into the CAA is equivalent to the Nd flux of seawater entering the CAA. Depending on the percentage of Nd removal during mixing with seawater, the impact of river water on the ε_{Nd} of seawater exiting the CAA could be modest (if 90% removal) or more significant (if $\ll$90% removal). CAA riverine discharge could add a climate-sensitive Nd isotopic signature to the seawater entering Baffin Bay, particularly if permafrost thaw results in a substantial increase in the dissolved and colloidal load of CAA rivers. If the state of permafrost and the abrasion of crystalline bedrock by ice sheets are important factors in controlling the discharge of dissolved Nd from continents to coastal waters, their climate sensitivity could imply temporal variability in the Nd isotopic composition of the North Atlantic. This would have implications for the use of ε_{Nd} for paleoceanographic reconstructions of water masses and warrants further investigation.

CRediT authorship contribution statement

Mélanie Grenier: Conceptualization, Methodology, Investigation, Validation, Visualization, Writing – original draft preparation. **Kristina A. Brown:** Conceptualization, Methodology (Endmember scaling approach, determination of pH and total alkalinity), Writing – reviewing & editing. **Manuel Colombo:** Conceptualization, Writing – reviewing & editing. **Moustafa Belhadj:** Investigation, Resources. **Isabelle Baconnais:** Investigation, Writing – reviewing & editing. **Viet Pham:** Methodology (SeaSLOW development). **Maureen Soon:** Investigation, Resources. **Paul G. Myers:** Methodology (marine flux determination), Writing – reviewing & editing. **Catherine Jeandel:** Writing – reviewing & editing. **Roger François:** Project administration, Supervision, Conceptualization, Methodology, Writing – reviewing & editing.

Declaration of competing interest

The authors declare that they have no known competing financial interests or personal relationships that could have appeared to influence the work reported in this paper.

Acknowledgements

We wish to acknowledge the assistance of the captain, officers and crew of the CCGS Amundsen during the research expedition. We also acknowledge, on the one hand, Aurélie Marquet, Camille Duquenoy and Jérôme Chmeleff and, on the other hand, Stephanie Mounic and Mathieu Benoit (Centre National de la Recherche Scientifique, GET) for their technical support on the ICP-MS and on the TIMS, respectively. For the model transports, we acknowledge Compute Canada (www.computecanada.ca). Finally, we thank the anonymous reviewers whose insightful comments and suggestions helped to improve the manuscript. The Canadian Arctic GEOTRACES project was funded by the Canadian research program NSERC CCAR. M. Grenier was supported by a European Union's Horizon 2020 research and innovation programme (Marie Skłodowska-Curie action, Grant Agreement 657853). The REE data set reported in this study is available on the GEOTRACES International Data Assembly Centre (www.bodc.ac.uk/geotraces/data/).

Appendix A. Supplementary material

Supplementary material related to this article can be found online at https://doi.org/10.1016/j.epsl.2021.117341.

References

Abbott, A.N., Haley, B.A., McManus, J., Reimers, C.E., 2015. The sedimentary flux of dissolved rare earth elements to the ocean. Geochim. Cosmochim. Acta 154, 186–200. https://doi.org/10.1016/j.gca.2015.01.010.

Alkire, M.B., Jacobson, A.D., Lehn, G.O., Macdonald, R.W., Rossi, M.W., 2017. On the geochemical heterogeneity of rivers draining into the straits and channels of the Canadian Arctic Archipelago. J. Geophys. Res., Biogeosci. 122, 2527–2547. https://doi.org/10.1002/2016JG003723.

Benoit, G., Rozan, T.F., 1999. The influence of size distribution on the particle concentration effect and trace metal partitioning in rivers. Geochim. Cosmochim. Acta 63, 113–127. https://doi.org/10.1016/S0016-7037(98)00276-2.

Bolhar, R., Kamber, B.S., Moorbath, S., Fedo, C.M., Whitehouse, M.J., 2004. Characterisation of early Archaean chemical sediments by trace element signatures. Earth Planet. Sci. Lett. 222, 43–60. https://doi.org/10.1016/j.epsl.2004.02.016.

Brown, K.A., Williams, W.J., Carmack, E.C., Fiske, G., François, R., McLennan, D., Peucker-Ehrenbrink, B., 2020. Geochemistry of small Canadian Arctic rivers with diverse geological and hydrological settings. J. Geophys. Res., Biogeosci. 125, 1–21. https://doi.org/10.1029/2019JG005414.

Byrne, R.H., Kim, K.-H., 1990. Rare earth element scavenging in seawater. Geochim. Cosmochim. Acta 54, 2645–2656. https://doi.org/10.1016/0016-7037(90)90002-3.

Chupakov, A.V., Pokrovsky, O.S., Moreva, O.Y., Shirokova, L.S., Neverova, N.V., Chupakova, A.A., Kotova, E.I., Vorobyeva, T.Y., 2020. High resolution multi-annual riverine fluxes of organic carbon, nutrient and trace element from the largest European Arctic river, Severnaya Dvina. Chem. Geol. 538, 119491. https://doi.org/10.1016/j.chemgeo.2020.119491.

Colombo, M., Brown, K.A., De Vera, J., Bergquist, B.A., Orians, K.J., 2019. Trace metal geochemistry of remote rivers in the Canadian Arctic Archipelago. Chem. Geol. 525, 479–491. https://doi.org/10.1016/j.chemgeo.2019.08.006.

Colombo, M., Jackson, S.L., Cullen, J.T., Orians, K.J., 2020. Dissolved iron and manganese in the Canadian Arctic Ocean: on the biogeochemical processes controlling their distributions. Geochim. Cosmochim. Acta 277, 150–174. https://doi.org/10.1016/j.gca.2020.03.012.

Connolly, C.T., Cardenas, M.B., Burkart, G.A., Spencer, R.G.M., McClelland, J.W., 2020. Groundwater as a major source of dissolved organic matter to Arctic coastal waters. Nat. Commun. 11, 1–9. https://doi.org/10.1038/s41467-020-15250-8.

Elderfield, H., 1988. The oceanic chemistry of the rare-earth elements. Philos. Trans. R. Soc. Lond. Ser. A, Math. Phys. Sci. 325, 105–126. https://doi.org/10.1098/rsta.1988.0046.

Elderfield, H., Upstill-Goddard, R., Sholkovitz, E.R., 1990. The rare earth elements in rivers, estuaries, and coastal seas and their significance to the composition of ocean waters. Geochim. Cosmochim. Acta 54, 971–991. https://doi.org/10.1016/0016-7037(90)90432-K.

Frank, M., 2002. Radiogenic isotopes: tracers of past ocean circulation and erosional input. Rev. Geophys. 40. https://doi.org/10.1029/2000RG000094.

Frey, K.E., McClelland, J.W., 2009. Impacts of permafrost degradation on arctic river biogeochemistry. Hydrol. Process. 23, 169–182. https://doi.org/10.1002/hyp.7196.

Garrity, C.P., Soller, D.R., 2009. Database of the geologic map of North America—adapted from the map by J.C. Reed, Jr. and others, 2005. U.S. Geological Survey Data Series, vol. 424. USGS, Denver, CO, USA. https://pubs.usgs.gov/ds/424/.

Goldstein, S.J., Jacobsen, S.B., 1988. Rare earth elements in river waters. Earth Planet. Sci. Lett. 89, 35–47. https://doi.org/10.1016/0012-821X(88)90031-3.

Grenier, M., François, R., Soon, M., Rutgers van der Loeff, M., Yu, X., Valk, O., Not, C., Moran, S.B., Edwards, R.L., Lu, Y., Lepore, K., Allen, S.E., 2019. Changes in circulation and particle scavenging in the Amerasian Basin of the Arctic Ocean over the last three decades inferred from the water column distribution of geochemical tracers. J. Geophys. Res., Oceans 124, 9338–9363. https://doi.org/10.1029/2019JC015265.

Grenier, M., Jeandel, C., Lacan, F., Vance, D., Venchiarutti, C., Cros, A., Cravatte, S., 2013. From the subtropics to the central equatorial Pacific Ocean: neodymium isotopic composition and rare earth element concentration variations. J. Geophys. Res., Oceans 118, 592–618. https://doi.org/10.1029/2012JC008239.

Grivault, N., Hu, X., Myers, P.G., 2018. Impact of the surface stress on the volume and freshwater transport through the Canadian Arctic archipelago from a high-resolution numerical simulation. J. Geophys. Res., Oceans 123, 9038–9060. https://doi.org/10.1029/2018JC013984.

Hatje, V., Bruland, K.W., Flegal, A.R., 2014. Determination of rare earth elements after pre-concentration using NOBIAS-chelate PA-1®resin: method development and application in the San Francisco Bay plume. Mar. Chem. 160, 34–41. https://doi.org/10.1016/j.marchem.2014.01.006.

Holmes, R.M., McClelland, J.W., Peterson, B.J., Tank, S.E., Bulygina, E., Eglinton, T.I., Gordeev, V.V., Gurtovaya, T.Y., Raymond, P.A., Repeta, D.J., Staples, R., Striegl, R.G., Zhulidov, A.V., Zimov, S.A., 2012. Seasonal and annual fluxes of nutrients and organic matter from large rivers to the Arctic Ocean and surrounding seas. Estuar. Coast. 35, 369–382. https://doi.org/10.1007/s12237-011-9386-6.

Howe, J.N.W., Piotrowski, A.M., Rennie, V.C.F., 2016. Abyssal origin for the early Holocene pulse of unradiogenic neodymium isotopes in Atlantic seawater. Geology 44, 831–834. https://doi.org/10.1130/G38155.1.

Ingri, J., Öhlander, B., Widerlund, A., Andersson, P., Land, M., Gustafsson, Ö., 2000. Temporal variations in the fractionation of the rare earth elements in a boreal river; the role of colloidal particles. Chem. Geol. 166, 23–45.

Jeandel, C., Arsouze, T., Lacan, F., Téchiné, P., Dutay, J.C., 2007. Isotopic Nd compositions and concentrations of the lithogenic inputs into the ocean: a compilation, with an emphasis on the margins. Chem. Geol. 239, 156–164. https://doi.org/10.1016/j.chemgeo.2006.11.013.

Lacan, F., Jeandel, C., 2005. Neodymium isotopes as a new tool for quantifying exchange fluxes at the continent-ocean interface. Earth Planet. Sci. Lett. 232, 245–257. https://doi.org/10.1016/j.epsl.2005.01.004.

Lafrenière, M., Lamoureux, S., 2008. Seasonal dynamics of dissolved nitrogen exports from two High Arctic watersheds, Melville Island, Canada. Hydrol. Res. 39, 323–335. https://doi.org/10.2166/nh.2008.008.

Lewis, T., Lafrenière, M.J., Lamoureux, S.F., 2012. Hydrochemical and sedimentary responses of paired High Arctic watersheds to unusual climate and permafrost disturbance, Cape Bounty, Melville Island, Canada. Hydrol. Process. 26, 2003–2018. https://doi.org/10.1002/hyp.8335.

Li Yung Lung, J.Y.S., Tank, S.E., Spence, C., Yang, D., Bonsal, B., McClelland, J.W., Holmes, R.M., 2018. Seasonal and geographic variation in dissolved carbon biogeochemistry of rivers draining to the Canadian Arctic Ocean and Hudson Bay. J. Geophys. Res., Biogeosci. 123, 3371–3386. https://doi.org/10.1029/2018JG004659.

Mackie, R.A., Scoates, J.S., Weis, D., 2009. Age and Nd-Hf isotopic constraints on the origin of marginal rocks from the Muskox layered intrusion (Nunavut, Canada) and implications for the evolution of the 1.27 Ga Mackenzie large igneous province. Precambrian Res. 172, 46–66. https://doi.org/10.1016/j.precamres.2009.03.007.

McLennan, S.M., 2001. Relationships between the trace element composition of sedimentary rocks and upper and continental crust. Geochem. Geophys. Geosyst. https://doi.org/10.1029/2005GC001005.

Michel, C., Hamilton, J., Hansen, E., Barber, D., Reigstad, M., Iacozza, J., Seuthe, L., Niemi, A., 2015. Arctic Ocean outflow shelves in the changing Arctic: a review and perspectives. Prog. Oceanogr. 139, 66–88. https://doi.org/10.1016/j.pocean.2015.08.007.

Millero, F.J., 1979. The thermodynamics of the carbonate system in seawater. Geochim. Cosmochim. Acta 43, 1651–1661. https://doi.org/10.1016/0016-7037(79)90184-4.

Okulitch, A.V., 1991. Geology of the Canadian Arctic Archipelago, Northwest Territories and North Greenland.

Pearce, C.R., Jones, M.T., Oelkers, E.H., Pradoux, C., Jeandel, C., 2013. The effect of particulate dissolution on the neodymium (Nd) isotope and Rare Earth Element (REE) composition of seawater. Earth Planet. Sci. Lett. 369–370, 138–147. https://doi.org/10.1016/j.epsl.2013.03.023.

Pham, V., 2020. Traçage de l'empreinte lithogénique en mers de Corail et des Salomon: apport des terres rares et de la composition isotopique du néodyme. Université Toulouse 3.

Pierrot, D., Lewis, E., Wallace, D.W.R., 2006. MS excel program developed for CO2 system calculations. https://doi.org/10.3334/CDIAC/otg.CO2SYS_XLS_CDIAC105a.

Pokrovsky, O.S., Schott, J., 2002. Iron colloids/organic matter associated transport of major and trace elements in small boreal rivers and their estuaries (NW Russia). Chem. Geol. 190, 141–179. https://doi.org/10.1016/S0009-2541(02)00115-8.

Pokrovsky, O.S., Viers, J., Shirokova, L.S., Shevchenko, V.P., Filipov, A.S., Dupré, B., 2010. Dissolved, suspended, and colloidal fluxes of organic carbon, major and trace elements in the Severnaya Dvina River and its tributary. Chem. Geol. 273, 136–149. https://doi.org/10.1016/j.chemgeo.2010.02.018.

Pöppelmeier, F., Scheen, J., Blaser, P., Lippold, J., Gutjahr, M., Stocker, T.F., 2020. Influence of elevated Nd fluxes on the northern Nd isotope end member of the Atlantic during the early Holocene. Paleoceanogr. Paleoclimatol. 35. https://doi.org/10.1029/2020PA003973.

Pourret, O., Tuduri, J., 2017. Continental shelves as potential resource of rare earth elements. Sci. Rep. 7, 1–6. https://doi.org/10.1038/s41598-017-06380-z.

Rousseau, T.C.C., Sonke, J.E., Chmeleff, J., van Beek, P., Souhaut, M., Boaventura, G., Seyler, P., Jeandel, C., 2015. Rapid neodymium release to marine waters from lithogenic sediments in the Amazon estuary. Nat. Commun. 6, 7592. https://doi.org/10.1038/ncomms8592.

Stolpe, B., Guo, L., Shiller, A.M., 2013. Binding and transport of rare earth elements by organic and iron-rich nanocolloids in Alaskan rivers, as revealed by field-flow fractionation and ICP-MS. Geochim. Cosmochim. Acta 106, 446–462. https://doi.org/10.1016/j.gca.2012.12.033.

Stordal, M.C., Wasserburg, G.J., 1986. Neodymium isotopic study of Baffin Bay water: sources of REE from very old terranes. Earth Planet. Sci. Lett. 77, 259–272.

Tang, D., Warnken, K.W., Santschi, P.H., 2002. Distribution and partitioning of trace metals (Cd, Cu, Ni, Pb, Zn) in Galveston Bay waters. Mar. Chem. 78, 29–45. https://doi.org/10.1016/S0304-4203(02)00007-5.

Tepe, N., Bau, M., 2016. Behavior of rare earth elements and yttrium during simulation of Arctic estuarine mixing between glacial-fed river waters and seawater and the impact of inorganic (nano-)particles. Chem. Geol. 438, 134–145. https://doi.org/10.1016/j.chemgeo.2016.06.001.

Tepe, N., Bau, M., 2015. Distribution of rare earth elements and other high field strength elements in glacial meltwaters and sediments from the western Greenland Ice Sheet: evidence for different sources of particles and nanoparticles. Chem. Geol. 412, 59–68. https://doi.org/10.1016/j.chemgeo.2015.07.026.

Veizer, J., 1983. Chapter 8. Trace elements AND isotopes IN sedimentary carbonates. In: Reeder, R.J. (Ed.), Carbonates: Mineralogy and Chemistry. De Gruyter, Berlin, Boston, pp. 265–300.

Villeneuve, M.E., Relf, G., 1998. Tectonic setting of 2.6 Ga carbonatites in the Slave Province, NW Canada. J. Petrol. 39, 1975–1986. https://doi.org/10.1093/petroj/39.11-12.1975.

Wasserburg, G.J., Jacousen, S.B., DePaolo, D.J., McCulloch, M.T., Wen, T., 1981. Precise determination of Sm Nd ratios, Sm and Nd isotopic abundances in standard solutions. Geochim. Cosmochim. Acta 45, 2311–2323. https://doi.org/10.1016/0016-7037(81)90085-5.

Wilson, D.J., Crocket, K.C., van de Flierdt, T., Robinson, L.F., Adkins, J.F., 2014. Dynamic intermediate ocean circulation in the North Atlantic during Heinrich Stadial 1: a radiocarbon and neodymium isotope perspective. Paleoceanography 29, 1072–1093. https://doi.org/10.1002/2014PA002674.

Zhao, N., Oppo, D.W., Huang, K.F., Howe, J.N.W., Blusztajn, J., Keigwin, L.D., 2019. Glacial–interglacial Nd isotope variability of North Atlantic Deep Water modulated by North American ice sheet. Nat. Commun. 10, 1–10. https://doi.org/10.1038/s41467-019-13707-z.